Applied Catalysis A: General 407 (2011) 173–180

Contents lists available at SciVerse ScienceDirect

Applied Catalysis A: General

journal homepage: www.elsevier.com/locate/apcata

Kinetic study of the hydrogenation of p-nitrophenol to p-aminophenol over micro-aggregates of nano-Ni_2B catalyst particles

Firoozeh Taghavi[a,b], Cavus Falamaki[c,d,*], Alimemad Shabanov[a], Leila Bayrami[b], Amir Roumianfar[b]

[a] Research Institute of Geotechnological Problems of Oil, Gas and Chemistry, Azerbaijan Sate oil Academy, Baku, Azerbaijan
[b] Research and Development Department, Chlor Pars Co., P.O. Box 51335-1717, Tabriz, Iran
[c] Chemical Engineering Department, Amirkabir University of Technology, P.O. Box 15875-4413, Tehran, Iran
[d] Petrochemical Center of Excellence, Amirkabir University of Technology, P.O. Box 15875-4413, Tehran, Iran

ARTICLE INFO

Article history:
Received 14 May 2011
Received in revised form 20 August 2011
Accepted 21 August 2011
Available online 26 August 2011

Keywords:
Nickel boride
Hydrogenation
p-Aminophenol
p-Nitrophenol
Nano-catalyst

ABSTRACT

The present work concerns a thorough investigation of the performance of a nano-nickel boride catalyst for the direct hydrogenation of p-nitrophenol (PNP) to p-aminophenol (PAP) in a batch slurry reactor using ethanol as solvent. The effect of pH during the synthesis procedure on the properties of the as-synthesized catalyst has been investigated using FTIR, XRD, ICP and FESEM analysis. The synthesized catalyst shows a better activity with respect to Raney nickel. The effect of catalyst preparatory method on its activity has been investigated. The effect of reaction temperature (40–80 °C), PNP initial concentration (0.07–0.28 g mL^{-1}) and initial pressure (25–40 bar) on the reaction kinetics has been investigated. It has been shown that the kinetic behavior throughout the whole time domain could be reasonably predicted considering a single site mechanism with atomically adsorbed hydrogen and PNP adsorption as the controlling step.

1. Introduction

Recently, particular attention has been given to non-noble hydrogenation catalysts produced via metal salt reduction such as cobalt, cobalt boride, nickel boride and nickel cobalt boride [1–3]. Nickel and cobalt borides are among the most investigated catalysts. These compounds are gaining interest in the industrial production of H_2 from $NaBH_4$.

Among the various metal borides, nickel borides are regarded as potential industrial catalysts for hydrogenation reactions [4]. Ni–B alloy is a novel industrial catalyst famous for its high activity, low-cost and strong sulfur resistance in hydrogenation reactions [5]. The inclusion of boron in the nickel metal has also been reported to improve the resistance against thermal oxidation [6]. The application of nickel borides in the hydrogenation of aromatic nitro compounds, alkynes, alkenes, aldehydes, ketones, aliphatic nitro groups and nitriles has been the subject of numerous studies [7–26]. As far as the kinetics of hydrogenation of nitro aromatic compounds is concerned, the published works on the use of nickel borides as catalysts are restricted mainly to multi-step reactions using nitro aromatics as reactant [15,27]. Chen and Hsieh [15] reported a detailed work on the kinetics of the hydrogenation of nitrobenzene at 373 K using a nickel boride nano-particle catalyst. The stoichiometric chemical formula was determined as $Ni_{69.3}B_{30.7}$ without any phase identification. Liu et al. [27] reported an interesting investigation on the hydrogenation of p-chloronitrobenzene using nickel boride as catalyst and alcoholic solvents (methanol and ethanol). Based on ICP analysis, their nano-catalysts consisted of low boron nickel borides ($Ni_{14.38}B$, $Ni_{23.9}B$ and $Ni_{5.57}B$). They deduced that incorporating boron in the framework of Ni (Raney Nickel) results in an increase of the hydrogenation activity. It is presumed that the electron transfer from B atoms to Ni atoms in nickel boride catalysts enhances the intrinsic activity for the hydrogenation reaction [11].

The hydrogenation reaction of PNP to PAP using nickel boride catalysts is a new subject and the relevant open literature is scarce. Raney nickel, the most widely used industrial catalyst for this reaction, suffers the twin disadvantages of being moisture sensitive and pyrophoric [28,29]. On the other hand, commercially available Raney nickel catalysts not only catalyze the hydrogenation of nitro to amino group, but also catalyze the hydrogenation of the aromatic ring [30].

A recent work of Wen et al. [31] describes the production of nickel boride for the indirect hydrogenation (hydrazine used as the source of hydrogen) of PNP to PAP. The catalyst was not characterized properly and the reaction mechanism was not studied.

* Corresponding author at: Chemical Engineering Department, Amirkabir University of Technology, P.O. Box 15875-4413, Tehran, Iran. Tel.: +98 21 64 54 31 60; fax: +98 21 66 40 58 47.
E-mail address: c.falamaki@aut.ac.ir (C. Falamaki).

0926-860X/$ – see front matter © 2011 Elsevier B.V. All rights reserved.
doi:10.1016/j.apcata.2011.08.036

Rahman and Jonnalagadda [32] reported the hydrogenation of PNP using in situ synthesis of a nickel boride catalyst during the hydrogenation reaction by the addition of $NaBH_4$ to the reactants using methanol as solvent. The latter work lacks of any characterization of the claimed nickel boride catalyst produced during the reaction. The latter work also is a catalytic transfer hydrogenation reaction where hydrogen is supplied indirectly by one of the reactants.

A recent study of Liu et al. [33] reports the direct hydrogenation of PNP using a nickel boride catalyst supported on bohemite. They did not identify the nickel boride phase and did not report any elemental analysis of the boride catalyst. The latter work did not investigate the reaction mechanism, either.

The present work concerns a thorough investigation of the performance of a nickel boride catalyst for the direct hydrogenation of PNP to PAP in a batch slurry reactor using ethanol as solvent. The synthesized catalyst has been characterized by FESEM, BET, XRD, ICP and FTIR techniques. The catalytic activity of the synthesized catalyst has been compared with a Raney nickel catalyst. The effect of pH during the synthesis procedure on the activity of the catalyst has been studied. The effect of reaction temperature, PNP initial concentration, hydrogen initial pressure on the kinetics of the hydrogenation reaction has been investigated. Previous reaction modeling of PNP to PAP reaction over Pt/C and Raney nickel catalysts [34,35] considered only the "initial rate" data and lost a lot of additional information. This is while the evaluation of the initial rate is very sensitive and prone to errors. On the other hand, a reaction mechanism obtained based on only the initial rate data is not "forced" to predict correctly the species concentration during the whole reaction time domain. A kinetic expression for the reaction rate has been proposed that predicts reasonably well the experimental data throughout the temperature, pressure and initial PNP concentration range subject of the experimental work of this study. The advantage of the proposed model of the present work is that it aims at the prediction of the catalytic behavior over the whole time domain of each experiment series.

2. Materials and methods

2.1. Catalyst preparation

PNP was purchased from Anhui Bayi (China) with a purity of 99.5%. Sulfur free ethyl alcohol (96 wt.%) was purchased from Nasr Company (Iran). Sodium borohydride with a purity of 99% was purchased from Merck. Hydrogen with an assay of 99.999% and caustic soda (50 wt.%) were provided from Chlor Pars Company, Iran. Deionized water was used throughout the experiments.

To synthesize the nickel boride catalyst, 1.71 g $NaBH_4$ was dissolved in 25 mL of an aqueous solution of different pHs (0.05 M NaOH, 0.025 M NaOH, neutral and 0.05 M HCl). Then, the latter was added drop-wise to 25 mL of an aqueous solution of $NiCl_2$ (0.3 M) at RT under adequate agitation. The formation of the black precipitate was accompanied with the release of hydrogen gas. The latter precipitate was first washed with de-ionized water and afterwards with ethanol. The final product was kept under ethanol prior to use in the catalytic experiments. For comparative means, a Raney nickel catalyst was also produced. For this means, the precursor Ni–Al alloy (50 wt.% Ni, 50 wt.% Al) was prepared by arc-melting the pure constituent metals in a water-cooled copper hearth in an argon atmosphere. The alloy ingots were re-melted three to four times to ensure homogeneous compositions. The ingots were then crushed to an average size of ca. 5 mm. Finally, the latter were reacted with a 40 wt.% NaOH solution to leach the aluminum out at about 70 °C for several hours [36]. The porous solid product (Raney nickel) was washed with de-ionized water. The amounts of raw materials were chosen appropriately to obtain the same weight of final catalyst as in the case of nickel boride catalyst synthesis.

2.2. Catalytic tests

The catalytic hydrogenation of PNP to PAP was carried out in a stainless steel autoclave equipped with a special shaker. The particles used for the kinetic studies had been smaller than 50 μm. Size reduction was accomplished through wet milling of the product in ethanol media. The reactor was equipped with an external heating jacket (hot water circulation). The reactor was charged with 1 g catalyst for the kinetic analysis tests. Then, dry PNP (3.5 g) and ethanol as solvent (12.5–50 mL) were added to the reactor. Afterwards, the reactor was purged with a stream of nitrogen to remove air. The reactor was then heated to the reaction temperature (40–80 °C). Shaking (14–55 rpm) was commenced after reaching the reaction temperature. Afterwards, hydrogen was fed to the reactor (25–40 bar). The pressure of the reactor was monitored throughout the reaction. The pressure was monitored using a pressure gauge installed on the reactor system which had a precision of 0.05 bar.The reaction time varied between 20 min and 3 h.

The organic products were analyzed by a GC analyzer (Agilent 7890 Series, USA) equipped with a FID detector. Chromatographic separations were performed at 325 °C using an Agilent 19091j-413 30 m × 320 μm × 0.25 μm column and nitrogen as carrier gas at a flow rate of 1 mL min^{-1}. The melting point of the PAP product was measured using an Electrothermal 9100 apparatus (Digital Melting Point Co.).

2.3. Catalyst characterization

The catalyst was subjected to several analytical tests. ICP analysis was performed using an Integra XL (GBC) apparatus. For the latter analysis, the catalyst was washed with de-ionized water and dried at RT in a dessicator for 24 h. Field emission scanning electron microscopy (FESEM) analysis was performed using an S-4160 Hitachi instrument. X-ray diffraction analysis was performed using an X'pert (Philips) instrument. FTIR analysis was performed using a Tensor 27 (Brucker) instrument. Specific surface area was determined using an Autosorb-1 (Quanta Chrome) apparatus.

3. Results and discussion

3.1. Catalyst characterization

Fig. 1a and b shows the FESEM picture of the as-synthesized catalyst using a 0.05 M NaOH solution of $NaBH_4$. Although the agglomerates are quite large (Fig. 1a), they do disintegrate easily upon wet milling. According to Fig. 1b, the solid product is highly porous and consists of aggregates of nano-size primary particles (<100 nm). The primary particles have approximately a spherical morphology. Fig. 2a–c shows the effect of the pH on the morphology of the final product. Generally, the morphology is quasi-spherical using acidic and basic $NaBH_4$ solutions and the size of the primary particles is approximately the same. However, an abrupt change of morphology is observed using a neutral solution. Instead of an agglomerate of nano-particles, a continuous puffy structure has been formed.

Fig. 3 shows the effect of pH of the $NaBH_4$ solution on the FTIR spectrum of the final solid catalyst. It is observed that the spectrum is strongly affected by the pH of the initial solution. All the catalysts show a broad absorption band centered in the range of 3421–3453 cm^{-1} and a narrow band centered around 1631–1634 cm^{-1} corresponding to the hydrogen bonded O–H stretching and H–O–H bending vibrations, respectively [2]. The

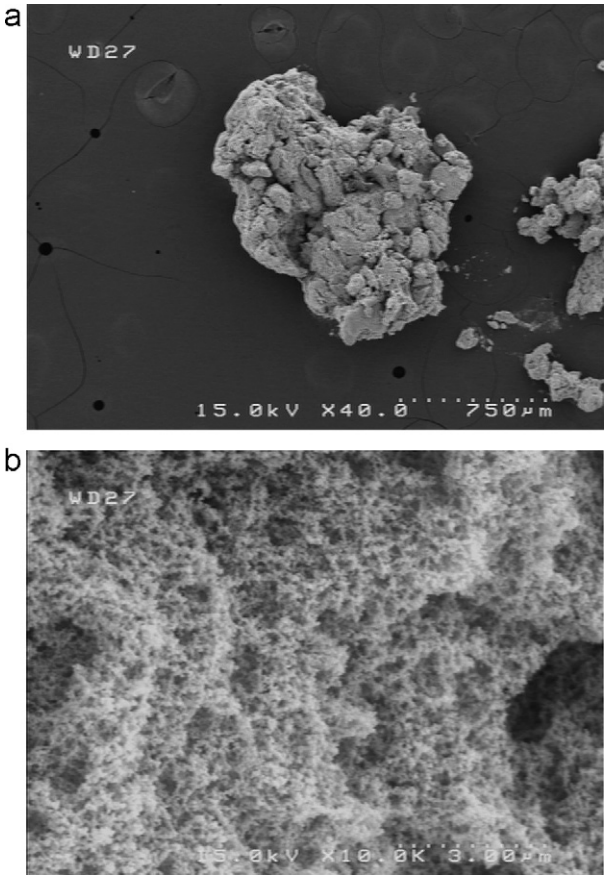

Fig. 1. FESEM pictures of the of the as-synthesized catalyst particle using a 0.05 M NaOH solution with different magnifications (a and b).

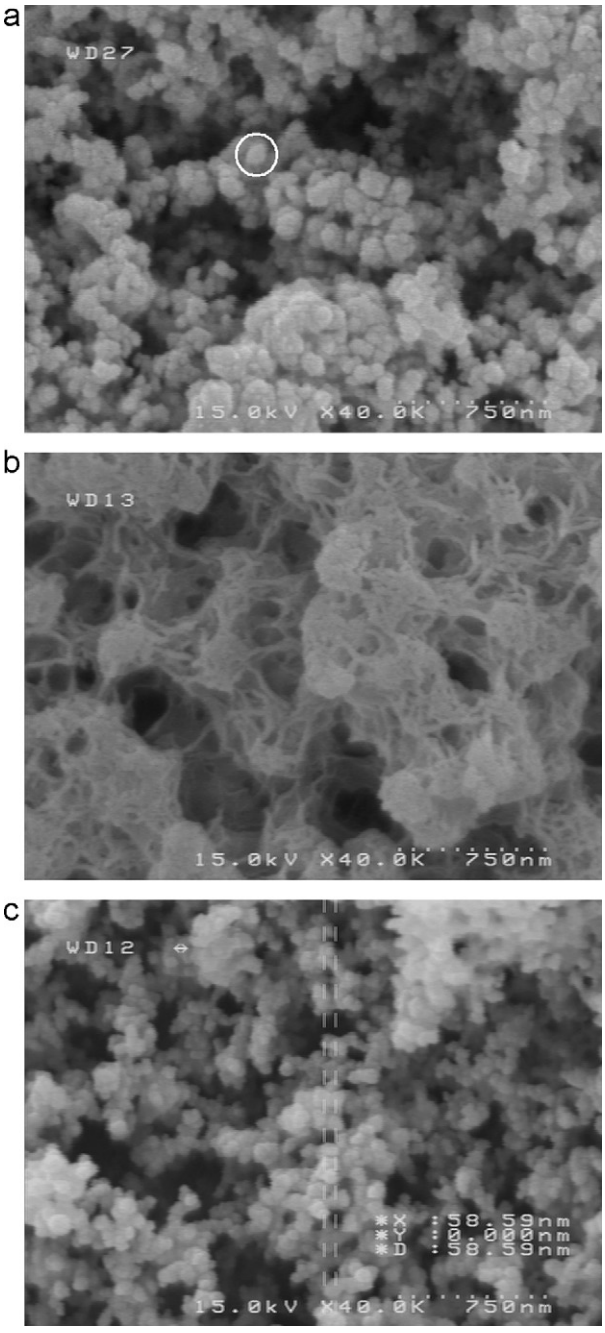

Fig. 2. The effect of $NaBH_4$ solution pH on the morphology of the catalyst primary particles: (a) using 0.05 M NaOH solution, (b) no additive, (c) 0.05 M HCl solution. Primary particles of approximate size of 60 nm and 58 nm have been indicated in (a–c).

main difference between the catalysts spectra lies in the wavenumber range of 400–1500 cm^{-1}. It should be recalled that the catalyst primary particles are nano-sized and therefore the effect of surface groups in the FTIR spectrum might be considerable. As we are concerned with 'nano-particles', it is noteworthy to allude to the fact that the phase structure might be different between the inner core and outer surface of the particles. The particles surface groups consist of B–O bonds of different length, depending on their parent structural unit (BO_2, BO_3 or BO_4) and irrespective of the composition of the inner core of the primary particles. The corresponding vibration mode and pertaining structural unit of each peak has been indicated in Fig. 3, based on the recent paper of Markova-Deneva [37]. Asymmetrical stretching vibration of BO_3 units appear in the range 1411–1454 cm^{-1} and 1266–1285 cm^{-1}, symmetrical stretching vibration of BO_2 units in the range of 1081–1100 cm^{-1}, symmetrical stretching vibration of BO_3 units at ca. 970 cm^{-1}, bending vibration of BO_4 units in the range of 631–670 cm^{-1}, bending vibration of BO_3 units at ca. 580 cm^{-1} and bending vibrations of BO_4 units in the range of 466–487 cm^{-1}. It is observed that peaks due to all the possible structural units of boron oxides are present in the spectrum of each of the catalysts. Considering the relative peak area in the range of 400–1500 cm^{-1} versus the area of the peak at around 1630 cm^{-1} (O–H vibration), it may be stated that the catalyst produced using no additive results in the least amount of boron inclusion in the outer shell of the catalyst particles. According to Fig. 3, the peaks due to BO_3 structural units prevail in all the samples. The sample produced in acidic media exhibits a slightly major content of BO_3 groups, eventually in the form of nickel borates such as $Ni_3(BO_3)_2$. At this stage, more insight may be gained by considering the complementary data obtained by the XRD and ICP techniques.

Fig. 4 shows the XRD pattern of the as-synthesized catalyst powders obtained immediately after short drying at room temperature of the sample previously maintained in ethanol. The amorphous structure of the powders is evident. However, distinct phases could be identified and have been indicated on the pertaining patterns. These include Ni_2B and $Ni_3(BO_3)_2$ phases with the corresponding JCPDS card numbers 48–1222 and 26–1284, respectively. It is observed that the highest crystallinity belongs to the catalyst produced in the acidic media. A clear decrease of crystallinity is observed increasing the basicity of the solution. Assigning a dominant phase to each of the XRD patterns is not possible at this stage. However, it is observed that the catalyst produced in the acidic medium has a detectable, albeit small, content of the $Ni_3(BO_3)_2$

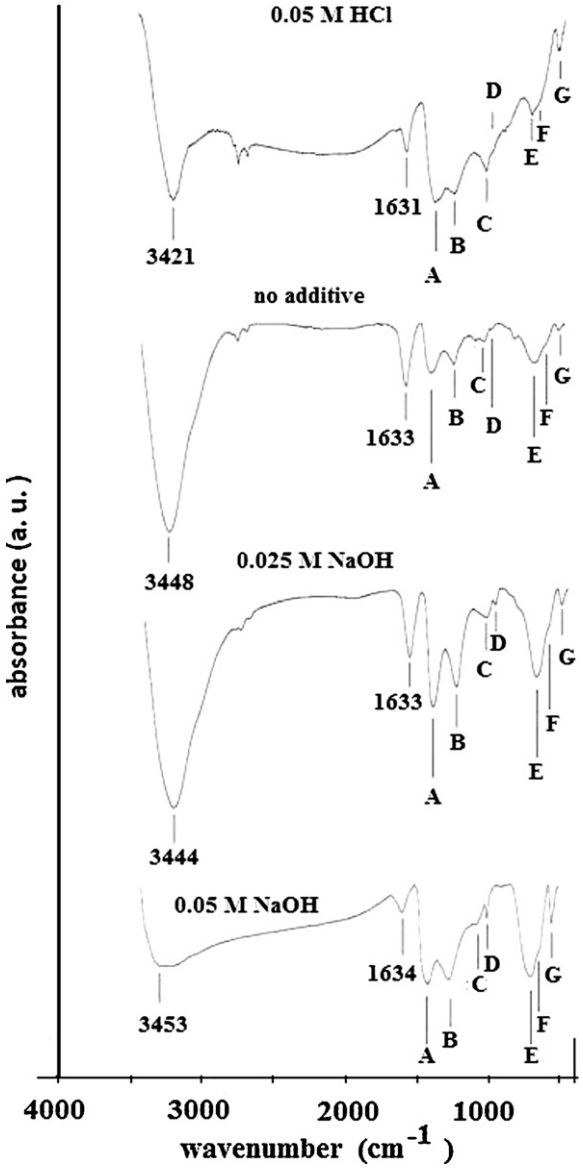

Fig. 3. FTIR pattern of the as-synthesized catalyst particle as a function of the pH of the $NaBH_4$ solution used. (A and B) Asymmetrical stretching vibration (BO_3 units), (C) symmetrical stretching vibration (BO_2 units), (D) symmetrical stretching vibration (BO_3 units), (E) bending vibration (BO_4 units), (F) bending vibration (BO_3 units) and (G) bending vibration (BO_4 units).

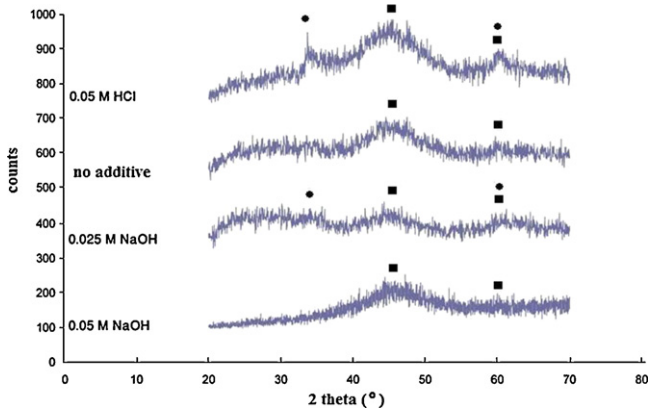

Fig. 4. XRD pattern of the as-synthesized catalyst particle as a function of the pH of the $NaBH_4$ solution used (■: Ni_2B, ●: $Ni_3(BO_3)_2$).

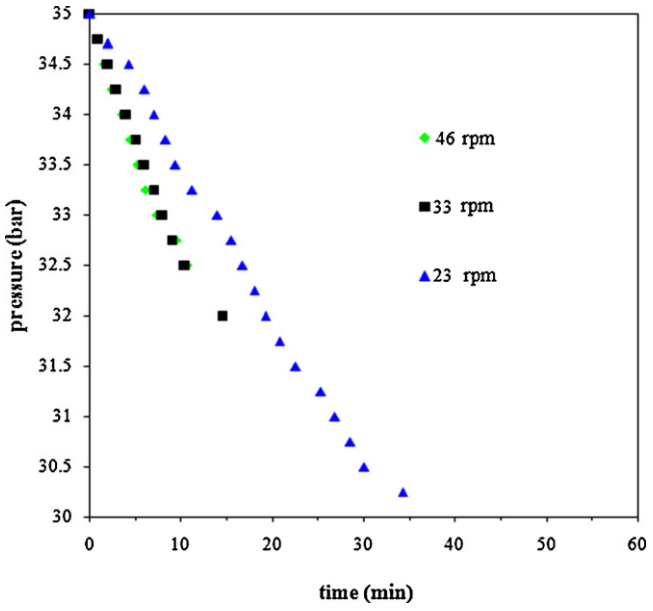

Fig. 5. System pressure variation versus reaction time as a function of agitation speed (H_2 initial pressure = 35 bar, initial PNP concentration = 0.14 g mL^{-1}, temperature = 80 °C) for catalyst BB1 (1 g).

phase. This is in accordance with the FTIR analysis discussed above, predicting a higher amount of included BO_3 units under acidic conditions.

The stoichiometric composition of the powders produced under different conditions has been determined using the ICP technique and is summarized in Table 1. It is clearly observed that increasing the acidity of the $NaBH_4$ solution results in the increase of the Ni content in the final powder. Based on the XRD and ICP analysis, it may be stated that the prevailing phase in all the samples is Ni_2B. As discussed before, no abrupt change in the FTIR spectrum or XRD pattern occurs when using a neutral $NaBH_4$ solution.

BET analysis showed a specific surface area (S) of 50.6 $m^2\,g^{-1}$. Considering a quasi-spherical geometry for the primary particles of the aggregates, their diameter is estimated to be 13.3 nm. For this calculation, the density of Ni_2B was taken as 8.9 g cm^{-3}. This is a reasonable assumption for nickel borides due to the relative large atomic weight of Ni with respect to B [8,13,14,27,38].

3.2. Kinetic experiments

A series of experiments were performed a priori to assess the effect of agitation speed on the reaction rate. The catalyst was produced using a 0.05 M NaOH aqueous solution of $NaBH_4$. For an initial PNP concentration of 0.14 g mL^{-1}, H_2 pressure of 35 bar and a reaction temperature of 80 °C, 4 experiments were run at 23, 33 and 46 rpm. Fig. 5 shows the pertaining results for the system pressure variation versus time. It is observed that increasing the agitation rate from 23 to 33 rpm, the rate of hydrogen consumption increases substantially. No significant increase in the rate is experienced by increasing the agitation rate from 33 to 46 rpm. It might be stated that an agitation speed of 46 rpm is approximately deprived of liquid phase diffusional resistances. Accordingly, all the kinetic experiments have been performed using an agitation speed of 46 rpm to ensure the absence of liquid phase transport resistances. As the size of Ni_2B micro-agglomerates used for the kinetic studies had been smaller than 50 μm, it is presumed that intraparticle diffusional resistance is negligible [34,35]. Therefore, the experimental kinetic data obtained in the following sections may

Table 1
Chemical composition of as-synthesized catalysts obtained by ICP analysis.

Name of catalyst[a]	Concentration of acid/base of the $NaBH_4$ solution	Raw chemical formula of as-synthesized catalyst	Catalytic activity as initial rate (bar min^{-1})[b]	Reaction time for 99% conversion of PNP (min)[b]
RN	–	Ni		60
A1	0.050 M HCl	$Ni_{2.00}B$	0.25	
A2	0.050 M HCl	$Ni_{2.16}B$		
N1	No acid/base	$Ni_{1.97}B$	0.17	
N2	No acid/base	$Ni_{1.97}B$		
B1	0.025 M NaOH	$Ni_{1.90}B$	0.23	
B2	0.025 M NaOH	$Ni_{1.95}B$		
BB1	0.050 M NaOH	$Ni_{1.85}B$	0.22	20
BB2	0.050 M NaOH	$Ni_{1.85}B$		

[a] The catalyst is produced by the dissolution of 1.71 g $NaBH_4$ in 25 mL of an aqueous solution with the concentration of acid (HCl), base (NaOH) shown in the second column. No acid/base means that it was dissolved in de-ionized water.
[b] Reaction temperature = 80 °C, initial pressure = 40 bar and PNP initial concentration = 0.14 g cm^{-3}.

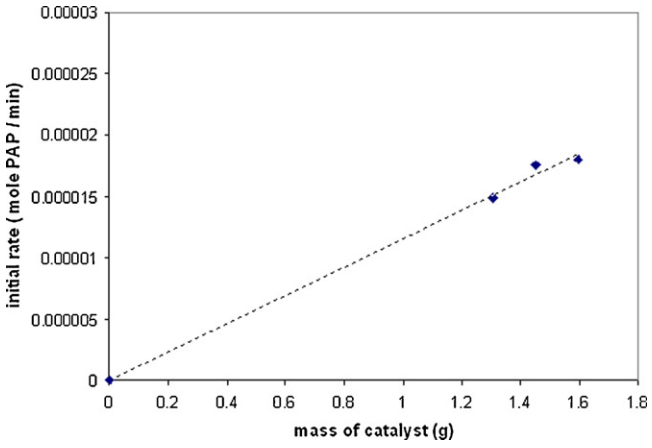

Fig. 6. The initial rate (mol PAP produced min^{-1}) as a function of mass catalyst BB1 used for a reaction temperature of 50 °C, PNP initial concentration of 0.14 g mL^{-1} and initial hydrogen pressure of 25 bar.

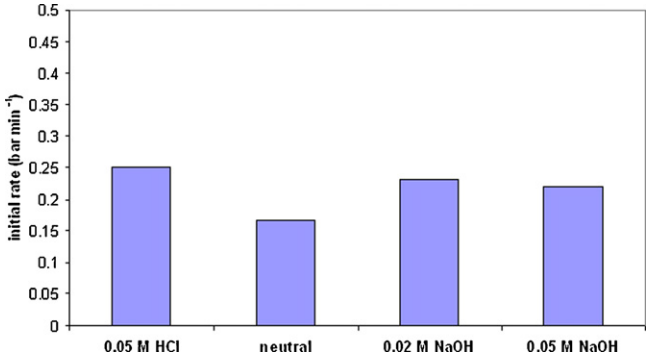

Fig. 7. The effect of the synthesis procedure on the initial rate of pressure change for an initial pressure of 40 bar, reaction temperature 80 °C and PNP concentration of 0.14 g mL^{-1}.

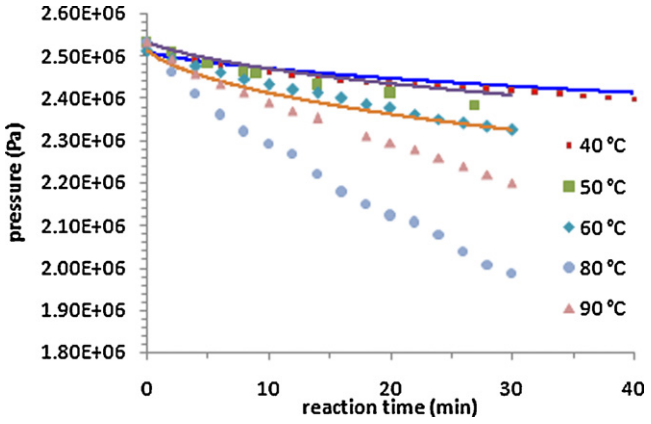

Fig. 8. Pressure variation with reaction time at a reaction temperature of: 40, 50, 60, 80 and 90 °C. Experimental conditions: hydrogen initial pressure 25 bar, agitation speed 45 rpm and initial PNP concentration 0.14 g cm^{-3}, 1 g catalyst BB1. Bold lines correspond to the simulated data.

be regarded to represent intrinsic reaction kinetics and will be used for the modeling studies.

To ascertain the absence of any gas–liquid mass transfer resistance, a series of tests were performed using different catalyst loadings. Fig. 6 shows the initial rate (mol PAP min^{-1}) as a function of mass catalyst used for a reaction temperature of 50 °C, PNP initial concentration of 0.14 g mL^{-1} and initial hydrogen pressure of 25 bar. The relationship is approximately linear, confirming the absence of the aforementioned resistance. It should be emphasized that in evaluating the reaction rate, the partial pressure of the solvent in the gas phase has been reasonably ignored. Recall that in each of the experiments the total pressure has been higher than 19 bar, which results in negligible solvent partial pressure, even at a reaction temperature of 80 °C.

Based on GC analysis of the final product, the purity of PAP was determined to be 99.5%. In addition, the melting point of the latter product was measured in the range of 186–188 °C which is in accordance with the British Pharmacopoeia standard (186 °C for 95% purity). These results show that side reactions, if any, are negligible.

A series of preliminary tests were run to observe the effect of the synthesis procedure on the initial rate of pressure change for an initial pressure of 40 bar, reaction temperature 80 °C and PNP concentration of 0.14 g mL^{-1}. The results are shown in Fig. 7. It is observed that irrespective of the concentration of acid or base, the catalyst shows a high activity. The least activity is observed using a neutral $NaBH_4$ solution while a meaningful difference between the other synthesis methods does not exist. The average TOF of the catalyst produced under basic or acidic conditions is ca. 7.58×10^{-5} mol PAP min^{-1} (g catalyst)$^{-1}$ for a reaction temperature of 80 °C.

3.2.1. *Effect of temperature, PNP initial concentration and hydrogen initial pressure*

To study the effect of reaction temperature, experiments were carried out in a temperature range of 40–90 °C for hydrogen initial pressure of 25 bar, agitation speed of 46 rpm and initial PNP concentration of 0.14 g mL^{-1}. The catalyst was synthesized using a 0.05 M NaOH aqueous solution of $NaBH_4$. The results are shown in Fig. 8.

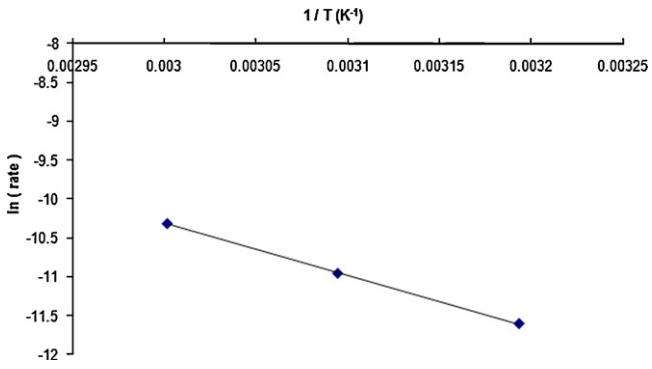

Fig. 9. Arrhenius plot of the experimental initial rates in 40–60 °C temperature range. Experimental conditions: hydrogen initial pressure 25 bar, agitation speed 45 rpm and initial PNP concentration 0.14 g cm^{-3}, 1 g catalyst (BB1 sample).

It is observed that the reaction rate increases with increasing temperature in the span of 40–80 °C. However, the reaction proceeds with a smaller rate at 90 °C when compared to 80 °C. This phenomenon may be attributed to (a) significant reduction of hydrogen solubility at 90 °C and/or (b) change of reaction mechanism in the temperature range of 80–90 °C. In other words, as far as PAP productivity is concerned, it seems that an optimum reaction temperature exists.

Considering the temperature range of 40–60 °C, the initial reaction rates have been evaluated and the corresponding Arrhenius plot has been drawn (Fig. 9). Accordingly, the activation energy has been estimated to be 55.7 kJ mol^{-1}. No data regarding the activation energy of PNP to PAP hydrogenation reaction over nickel boride catalysts has been reported in open literature so far. The values of 80 and 33.5 kJ mol^{-1} have been reported for the hydrogenation of p-chloronitrobenzene on a nano-size nickel boride catalyst [27] and lanthanum promoted nickel boride catalyst [32], respectively. This is while an activation energy of 50 kJ mol^{-1} has been reported for the hydrogenation of nitrobenzene over nickel boride catalysts [30]. Using a carbon supported Pd catalyst, Choudhary et al. [34] reported an activation energy of 70 kJ mol^{-1} for the hydrogenation of o-nitrophenol to o-aminophenol. Bawane and Sawant [35] reported a value of 47 kJ mol^{-1} for the hydrogenation of PNP to PAP using a Raney nickel catalyst.

Fig. 10 shows the effect of initial PNP concentration on the reaction kinetics for an initial pressure of ca. 25 bar and a reaction temperature of 40 °C. It is observed that increasing the concentration from 0.07 to 0.14 g mL^{-1} results in a slight increase of the reaction rate. It should be noted that the initial pressure in both cases was 24.7 bar. Further increase of the PNP initial concentration to 0.28 mL^{-1} actually results in further increase of the reaction rate. This is difficult to visualize at a first glance as the initial pressure had been 25.0 bar and therefore we have an upward shift of the curve due to an initial overpressure of 0.3 bar.

Fig. 11 shows the effect of initial hydrogen pressure (25, 30 and 40 bar) on the rate of hydrogen consumption as a function of time at a reaction temperature of 60 °C and initial PNP concentration of 0.14 g mL^{-1}. The initial reaction rate may be calculated to be 2.29×10^{-5}, 2.10×10^{-5} and 1.79×10^{-5} mol PAP min^{-1} for initial pressures 25, 30 and 40 bar, respectively. It is observed that the initial rate decreases as the pressure is increased. Such a phenomenon may be explained based on a proper reaction mechanism. This is the subject of the next discussion.

3.2.2. Mathematical modeling

Several models have been reported so far in the open literature for the PNP to PAP catalytic hydrogenation reaction. Choudhary et al. [34] bring a list of 8 different Hougen-Watson-type plausible

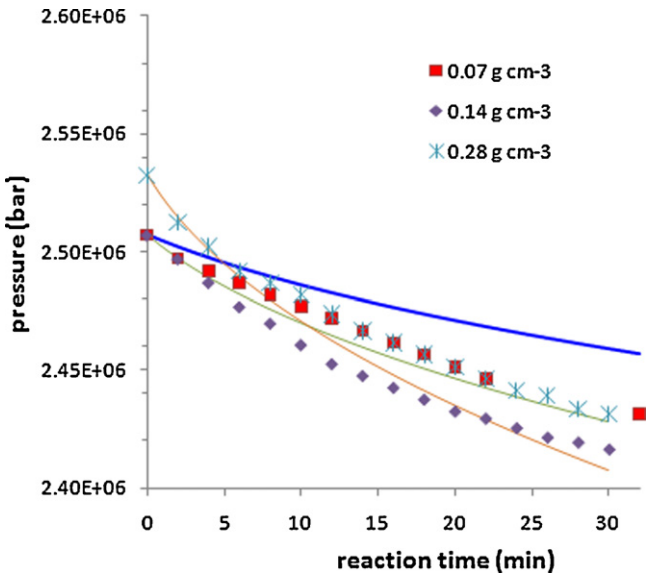

Fig. 10. The effect of time on stream of on the pressure variation at several initial PNP concentrations (in g cm^{-3}). Experimental conditions: hydrogen initial pressure ca. 25 bar, reaction temperature 40 °C, 1 g catalyst (BB1 sample). Bold lines correspond to the simulated data.

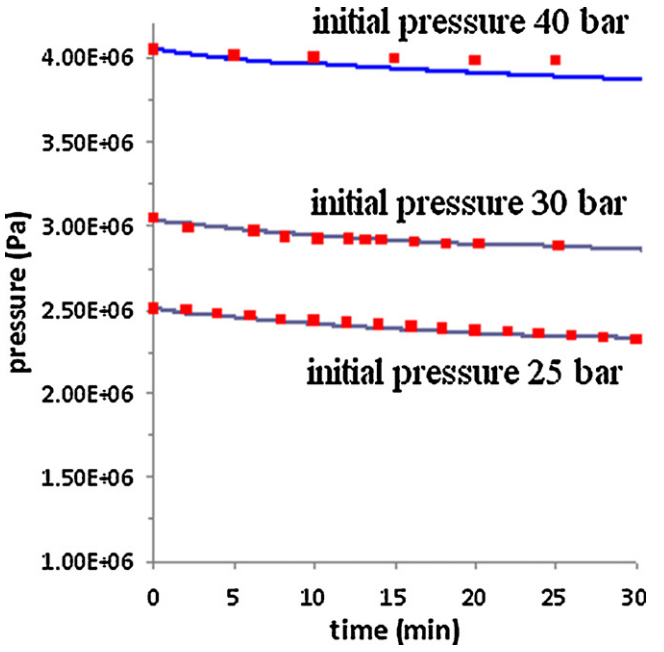

Fig. 11. The effect of initial hydrogen pressure on the variation of total pressure with reaction time. Experimental conditions: reaction temperature 60 °C, initial PNP concentration of 0.14 g mL^{-1}, 1 g catalyst (BB1 sample).

models for the latter reaction over Pt/carbon catalysts. They concluded that a single site mechanism could give the best fit of the experimental data for a reaction temperature range of 20–55 °C. Their model considered surface reaction as controlling while all the reaction species were molecularly adsorbed.

$$r_0 = \frac{k_3 K_{PNP} K_{H_2}^3 C_{PNP} C_{H_2}^3}{(1 + K_{PNP} C_{PNP} + K_{H_2} + C_{H_2} + K_{PAP} C_{PAP} + K_W C_W)^4} \quad (1)$$

where r_0 is the initial rate (mol PAP min^{-1} mL^{-1}), k_i is the specific reaction rate constant (i = 1,2,3,...), C_{H_2} the concentration of H_2 in the liquid phase (mol mL^{-1}), C_{PNP} the concentration of PNP in the liquid phase (mol mL^{-1}), C_{PAP} the concentration of PAP in the liquid

phase (mol mL^{-1}), C_W the concentration of water in the liquid phase (mol mL^{-1}), K_{H_2} the adsorption coefficient of H_2 (mL mol^{-1}), K_{PNP} the adsorption coefficient of PNP (mL mol^{-1}), K_{PAP} the adsorption coefficient of PAP (mL mol^{-1}) and K_W the adsorption coefficient of water (mL mol^{-1}).

Bawane and Sawant [35] present a list of 9 Langmuir–Hinshelwood possible models for the PNP hydrogenation reaction over Raney nickel catalysts. The catalyst used in the latter work is more close to the one subject of the present study. They also concluded that a single site mechanism could result in the best fitting of the experimental data for a reaction temperature range of 50–70 °C. However, their model considered atomic adsorption of H_2 and molecular adsorption of the other species. In addition, they considered again the surface reaction as being the controlling step. Their model is as follows:

$$r_0 = \frac{k_1 K_{PNP} K_{H_2} C_{PNP} C_{H_2}^3}{(1 + K_{PNP} C_{PNP} + K_{H_2}^{1/2} C_{H_2}^{1/2})^7} \quad (2)$$

As outlined by Choudhary et al. [34], such models should be interpreted as semi-empirical ones, not really representing the reaction mechanism of the catalytic hydrogenation of PNP.

Applying the above kinetic expressions, we tried to fit the experimental data. We realized that the above models could not at all predict a correct trend of the curves over the whole temperature, pressure and initial PNP concentration ranges considered. Preliminary calculations showed that model (1) could predict reasonably the initial rate data. However, the latter clearly failed fitting the species concentration during the whole reaction time. For this reason, we appealed to other possible mechanisms (see [34,35]) and obtained a reasonable fitting of the data using only a single site mechanism where H_2 is adsorbed atomically and the adsorption of PNP (and not the reaction), is controlling. The pertinent kinetic expression is as follows:

$$r_0 = \frac{k_1 C_{PNP}}{(1 + \sqrt{K_{H_2} C_{H_2}} + K_{PAP} C_{PAP} + K_W C_W)} \quad (3)$$

At this point, it should be recalled that past works did only fit the data due to "initial rates", i.e., at time zero. We tried to cover all time domains in each of the reaction experiments. The simulated hydrogen pressure as a function of time was obtained by integrating rate expression (3) using a fourth order Runge–Kutta method. Hydrogen solubility in ethanol as a function of temperature and pressure was retrieved from the literature [39]. The bold lines in Figs. 8, 10 and 11 show the simulated results.

The initial guesses for the adsorption coefficients were taken from the work of Choudhary et al. [34]. The optimal mathematical correlations of the model parameters have been derived through minimizing the residual sum of squares as follows:

$$k_1 = 2.1 \times 10^7 \ \exp\left(\frac{47,350}{RT}\right) \quad (4)$$

$$K_{H_2} = 2.5 \times 10^3 \ \exp\left(\frac{21,500}{RT}\right) \quad (5)$$

$$K_{PAP} = 5.5 \times 101 \ \exp\left(\frac{21,000}{RT}\right) \quad (6)$$

$$K_W = 3.0 \times 10^3 \ \exp\left(\frac{10,150}{RT}\right) \quad (7)$$

Concerning the effect of reaction temperature, it is observed that the range of 40–60 °C could be fitted reasonably. However, the model deviates significantly from the experimental data when applied to a reaction temperature range of 80–90 °C. We attribute the latter case mainly to a change of dominant mechanism, as the reduction of hydrogen solubility had been included during the calculations. The model predicts an activation energy of 47.35 kJ mol^{-1}, which is ca. 15% smaller than that obtained considering solely the experimental initial rates (55.7 kJ mol^{-1}).

Considering the effect of system pressure on the reaction kinetics, it observed that a reasonable prediction of the experimental data could be obtained using expression (3) for the reaction rate. The prediction of the effect of initial PNP concentration on the reaction kinetics is less accurate, but still reasonable (Fig. 10).

3.3. Comparison with Raney nickel catalyst

As a final step, two experiments were performed to compare the activity of the nickel boride catalyst with respect to conventional Raney nickel. As mentioned in the experimental section, the same weight of catalyst was used for each experiment. The experiments were run at a temperature of 80 °C, PNP initial concentration of 0.14 g mL^{-1} and initial hydrogen pressure of 40 bar. The time duration for complete conversion (>99%) of PNP was measured to be 20 and 60 min for the nickel boride and Raney nickel catalysts, respectively. The Ni_2B catalyst showed a significant better performance. Such an enhancement in catalytic activity may be attributed to an increased electron density of the nickel atom due to boron electron donation [40] leading to a higher intrinsic activity [11]. Boron alloying has also been reported to result in less poisoning of nickel catalytic sites by amine groups [41].

4. Conclusions

Micro-aggregates (<50 μm) of nano-Ni_2B particles have been successfully synthesized and used as PNP to PAP hydrogenation catalysts in a batch slurry reactor. The catalyst exhibits an increasing activity in the temperature range of 40–80 °C. A substantial reduction of the catalyst activity is observed in the temperature range 80–90 °C. This phenomenon has been attributed to the change of the reaction mechanism at temperatures higher than 80 °C. The activation energy in the temperature range of 40–60 °C had been calculated to be 55.7 kJ mol^{-1}.

The pH of the $NaBH_4$ solution influences the functional groups on the surface of the catalyst.

In this way, acid conditions seem to enhance mostly the incorporation of boron atoms as BO_3 structural units on the surface of the particles. The catalytic activity is only slightly enhanced using acid conditions while it is substantially decreased when using neutral conditions.

The catalytic behavior could be reasonably modeled using a single site mechanism based on atomic adsorption of H_2 and PNP adsorption as controlling step.

The nickel boride catalyst synthesized in this paper shows a catalytic performance better to that achieved over a Raney nickel catalyst.

Acknowledgement

This study was supported by the Chlor Pars Co., Tabriz, Iran.

References

[1] W. Ye, H. Zhang, D. Xu, L. Ma, B. Yi, J. Power Sources 164 (2007) 544–548.
[2] J.C. Ingersoll, N. Mani, J.C. Thenmozhiyal, A. Muthaiah, J. Power Sources 173 (2007) 450–457.
[3] C.M. Kaufman, B. Sen, J. Chem. Soc. Dalton Trans. 2 (1985) 307–331.
[4] H.C. Brown, C.A. Brown, J. Am. Chem. Soc. 85 (1963) 1003–1005.
[5] C. Luo, W.N. Wang, M.H. Qiao, K.N. Fan, J. Mol. Catal. A: Chem. 184 (2002) 379–386.
[6] Y.N. Bekish, T.V. Gaevskaya, L.S. Tsybulskaya, G.Y. Lee, M. Kim, Prot. Met. Phys. Chem. Surf. 4 (2010) 325–331.
[7] Y.Z. Chen, Y.C. Chen, Appl. Catal. A: Gen. 115 (1994) 45–57.
[8] Y.C. Chen, C.S. Tan, J. Supercrit. Fluids 41 (2007) 272–278.
[9] H. Li, Y. Xu, H. Yang, F. Zhang, H. Li, J. Mol. Catal. A, Chem. 307 (2009) 105–114.

[10] H. Li, J. Zhang, H. Li, Catal. Commun. 8 (2007) 2212–2216.
[11] Y.C. Liu, Y.W. Chen, Ind. Eng. Chem. Res. 45 (2006) 2973–2980.
[12] W.J. Wang, J.H. Shen, Y.W. Chen, Ind. Eng. Chem. Res. 45 (2006) 8860–8865.
[13] S.P. Lee, Y.W. Chen, J. Mol. Catal. A: Chem. 152 (2000) 213–223.
[14] D.J. Collins, A.D. Smith, B.H. Davis, Ind. Eng. Chem. Prod. Res. Dev. 21 (2) (1982) 279–281.
[15] Y.W. Chen, T. Hsieh, J. Nanopart. Res. 4 (2002) 455–461.
[16] H. Li, Q. Zhao, Y. Wan, W. Dai, M. Qiao, J. Catal. 244 (2006) 251–254.
[17] S. Ge, Z. Wu, M. Zhang, W. Li, K. Tao, Ind. Eng. Chem. Res. 45 (2006) 2229–2234.
[18] Z. Wu, M. Zhang, W. Lia, S. Mu, K. Tao, J. Mol. Catal. A: Chem. 273 (2007) 277–283.
[19] Z. Jiang, H. Yang, Z. Wei, Z. Xiea, W. Zhonga, S. Wei, Appl. Catal. A: Gen. 279 (2005) 165–171.
[20] H. Luo, W. Liu, Catal. Commun. 11 (2010) 803–807.
[21] H. Li, S. Zhang, H. Luo, Mater. Lett. 58 (2004) 2741–2746.
[22] M. Wu, W. Li, M. Zhang, K. Tao, Acta Phys.: Chim. Sin. 23 (2007) 1311–1315.
[23] J. Fang, X. Chen, B. Liu, S. Yan, M. Qiao, H. Li, J. Catal. 229 (2005) 97–104.
[24] Y. Hou, Y. Wang, Z. Mi, J. Mater. Sci. 40 (2005) 6585–6588.
[25] S. Caddick, D.B. Judd, A.K. de, K. Lewis, M.T. Reich, M.R.V. Williams, Tetrahedron 59 (2003) 5417–5423.
[26] H. Li, Y. Wu, J. Zhang, W. Dai, M. Qiao, Appl. Catal. A: Gen. 275 (2004) 199–206.
[27] Y.C. Liu, C.Y. Huang, Y.W. Chen, J. Nanopart. Res. 8 (2006) 223–234.
[28] S. Xu, X. Xi, J. Shi, S. Cao, J. Mol. Catal. A: Chem. 160 (2000) 287–292.
[29] K. Koprivova, L. Cerveny, Res. Chem. Intermed. 34 (2008) 93–101.
[30] Y. Du, H. Chen, R. Chen, N. Xu, Appl. Catal. A: Gen. 277 (2004) 259–264.
[31] H. Wen, K. Yao, Y. Zhang, Z. Zhou, A. Kirschning, Catal. Commun. 10 (2009) 1207–1211.
[32] A. Rahman, S.B. Jonnalagadda, Catal. Lett. 123 (2008) 264–268.
[33] H. Liu, J. Deng, W. Li, Catal. Lett. 137 (2010) 261–266.
[34] V.R. Choudhary, M.G. Sane, S.S. Tambe, Ind. Eng. Chem. Res. 37 (1998) 3879–3887.
[35] S.P. Bawane, S.B. Sawant, Appl. Catal. A: Gen. 293 (2005) 162–170.
[36] B.H. Liu, Q. Li, Int. J. Hydrogen Energy 33 (2008) 7385–7391.
[37] I. Markova-Deneva, J. Univ. Chem. Technol. Metal. 45 (2010) 351–378.
[38] L.F. Chen, Y.W. Chemn, Ind. Eng. Chem. Res. 45 (2006) 8866–8873.
[39] V.R. Choudhary, M.G. Sane, H.G. Vadnaonkar, J. Chem. Eng. Data 31 (1986) 294–296.
[40] L. Li, Q. Liang, A. Zhang, Chin. J. Catal. 28 (2007) 1031–1034.
[41] H. Li, Q. Zhao, H. Li, J. Mol. Catal. A: Chem. 285 (2008) 29–35.